Available online at www.sciencedirect.com
SCIENCE DIRECT®
Journal of Hydrology 297 (2004) 1–21
Journal of Hydrology
www.elsevier.com/locate/jhydrol

Modeling erosion and overbank deposition during extreme flood conditions on the Carson River, Nevada

R.W.H. Carroll[a,*], J.J. Warwick[a], A.I. James[b], J.R. Miller[c]

[a]*Division of Hydrologic Sciences, Desert Research Institute, 2215 Raggio Parkway, Reno, NV 89512-1095, USA*
[b]*Department of Environmental Engineering Sciences, University of Florida, Gainesville, FL 32611-6450, USA*
[c]*Department of Geosciences and Natural Resource Management, Western Carolina University, Cullowhee, NC 28723, USA*

Received 5 June 2002; revised 15 March 2004; accepted 1 April 2004

Abstract

The Carson River in west-central Nevada is one of the most mercury contaminated fluvial systems in North America. Most of its mercury is affiliated with channel bank material and floodplain deposits, with the movement of mercury through this system being highly dependent on sediment transport processes, particularly during overbank flows. To simulate these extreme situations, a United States Environmental Protection Agency (US EPA) hydrodynamic model (RIVMOD) was modified to include the 'divided channel approach' to estimate floodplain depths and velocities. The RIVMOD code was also augmented to allow dynamic width increases in the channel. Calibrated bank erosion functions, developed for the US EPA water quality model (WASP5), suggest that bank erosion is significantly greater at flows above bankfull discharge when compared to flows confined to the main channel. Verification of the bank erosion model matched observed width increases in 7 out of 10 reaches, with general trends matched in two of the remaining three reaches. Results also indicate that a single major flood event is responsible for nearly 87% of the total mass eroded during the period from 1991 to 1997. Overbank deposition was modeled using separate functions for coarse suspended sediment and washload material. Overbank deposition results are also in good agreement with observed values.

Keywords: Bank erosion; Overbank deposition; Numeric simulation; Extreme flood

1. Introduction

The United States Environmental Protection Agency (US EPA) designated the Carson River as part of a Superfund site in 1991 due to contamination by mercury. It is estimated that approximately 6.36×10^6 kg (7000 tons) of residual mercury is now distributed throughout the river's bank sediments and floodplain deposits (Miller et al., 1998; Smith and Tingley, 1998). It has also been found that more than 95% of the mercury transported in the Carson River is affiliated with particulate matter (Bonzongo et al., 1996). During January 1997 a rare, high-magnitude flood generated significant geomorphic change and resulted in an estimated 200,000 tons of sediment and 3,000 lbs of mercury to be transported downstream into Lahontan Reservoir (Hoffman and Taylor, 1998).

* Corresponding author. Tel.: +1-775-746-2496; fax: +1-775-673-7363.
E-mail address: rcarroll@dri.edu (R.W.H. Carroll).

0022-1694/$ - see front matter © 2004 Elsevier B.V. All rights reserved.
doi:10.1016/j.jhydrol.2004.04.012

These quantities far exceed the amount of sediment and mercury transported in the decade prior to the flood. Consequently, any useful model of mercury transport in the Carson River system requires an accurate simulation of bank erosion and floodplain sedimentation mechanisms during extreme flood events.

Examination of current bank erosion models (e.g. Darby and Thorne, 1996, CCHEBank, RIPA, SREAM2, WIDTH) was conducted by ASCE Task Committee on Hydraulics, Bank Mechanics and Modeling of River Width Adjustment (1998). Both this task committee, and Darby (1998), acknowledge that bank erosion processes are only understood enough for tentative width predictions. Furthermore, these high-resolution models are seriously constrained by the lack of field data for calibration and verification. It is also noted that there is no single, universal model of width adjustment that is applicable for all scenarios and that rarely are predictive channel erosion models used at the large spatial (80 km stream reach) and temporal scales (7 years) needed for this project.

With respect to modeling overbank deposition, many attempts have been made to characterize short-term floodplain dynamics. Analytical methods are presented by Pizzuto (1987), Howard (1992), and Walling and He (1997). More complex approaches to modeling overbank deposition include high-resolution, two-dimensional finite element models that incorporate overbank hydraulics as a function of topographical features (Bates et al., 1998; Gee et al., 1990; Nicholas and Walling, 1998). These models are capable of estimating velocity vectors and the subsequent floodplain sedimentation patterns. However, these models are constrained by lack of detailed hydraulic and topographic data necessary for model calibration and verification. As a result, these high-resolution models are limited to small model domains, straight channels, flat floodplains and/or hypothetical river/floodplain scenarios and are not appropriate for this study.

The modeling approach employed was developed to make use of readily available information. Specifically, USGS 7.5 min topographic maps of the study area were used to define floodplain and gross channel morphology (e.g. floodplain slopes and width, and longitudinal channel slope. Detailed channel cross-sections were not available for the large study domain, so average cross-sectional dimensions were obtained from direct field observations of a few locations deemed to be representative. These typical data constraints could not support a fully two- or three-dimensional modeling approach.

Previous modeling efforts of the Carson River have focused on sediment and mercury transport with river flows below bankfull discharge (Heim and Warwick, 1997; Carroll et al., 2000). Little attention has been given to the transport of material when flows over-top the confines of the main channel. Specific objectives of this study include (1) modify the hydrodynamic model RIVMOD (Hosseinipour and Martin, 1990) to estimate floodplain depths and velocities, (2) develop and verify a bank erosion function for flows above bankfull discharge, and (3) implement and evaluate a model for overbank deposition.

2. Site description

The Carson River flows eastward out of the Sierra Nevada Mountains just to the south of the Lake Tahoe Basin through a series of alluviated valleys and canyons until reaching the Carson Playa, a large hydrologically closed basin in the Carson Desert. Fig. 1 shows a map of the Carson River with several reference locations marked. The section of the Carson River under investigation extends from the USGS gaging station near Carson City, Nevada (CCG) downstream to the river's confluence with Lahontan Reservoir. The delta is located approximately 80 km from CCG and is approximately 10 km below the Fort Churchill gaging station (FCH).

Flow in the Carson River is typical of most semi-arid fluvial systems in that it is highly variable. Flow is predominately from snowmelt in the Sierra Nevada with peak discharge generally occurring in the spring with a sustained moderately high hydrograph. Catastrophic floods, such as the January 1997 flood, however, are generated with rare, rain-on-snow events that occur during the winter months. The summer and fall months are dominated by low flows and these flows can cease all together during extended periods of drought.

In 1859, the Comstock Lode was discovered near Virginia City, Nevada (see Fig. 1) and for the next

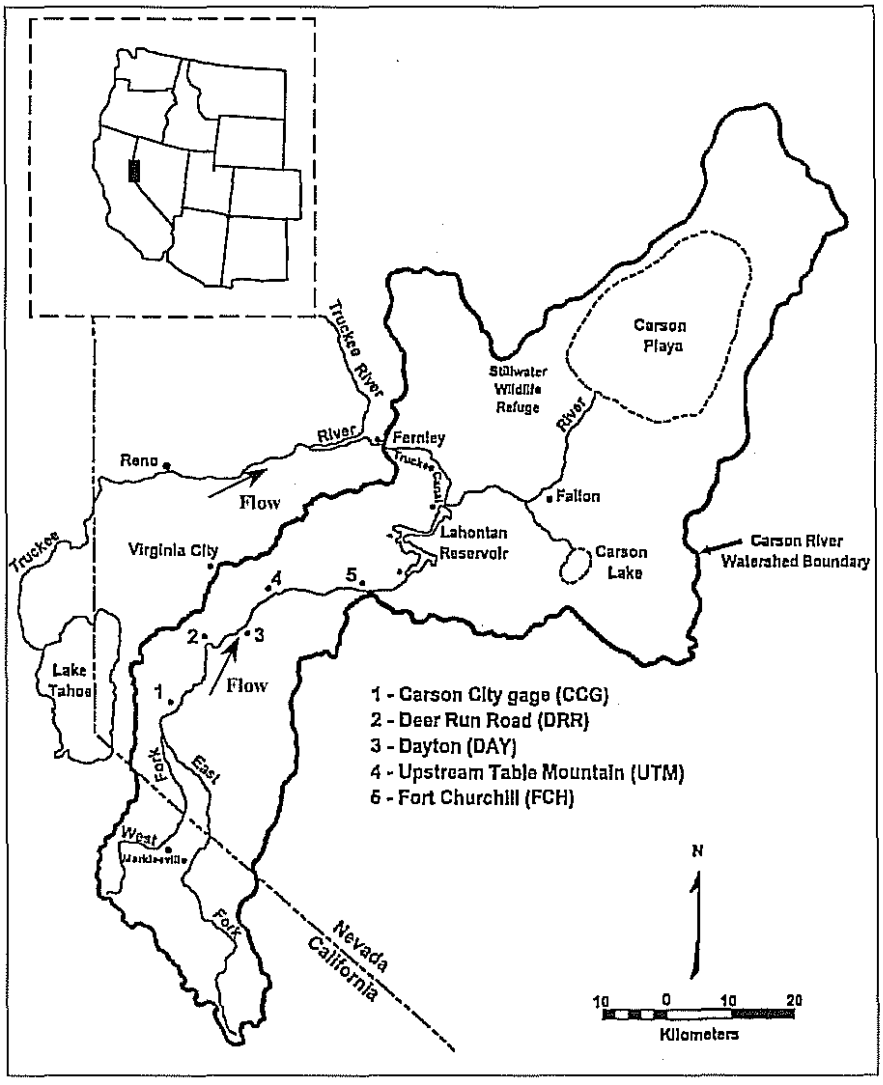

Fig. 1. The Carson River basin with reference locations marked. Upper left corner inset shows site location with respect to the western US.

three decades served as one of the worlds most productive gold- and silver-ore producing bodies in history. The massive influx of tailings materials, along with substantial sediment from clear cutting of the river's headwaters (timber used by the mills) caused the river to aggrade, experience lateral instabilities and meander abandonment. The decline of mining activity near the turn of the 20th century meant a drastic reduction in the sediment load. At this point, lateral instability was combined with downcutting (Miller et al., 1998). Today, the meandering river is entrenched with steep sides of complexly structured alluvial fill. Vegetation consists of a very limited riparian canopy, mostly of cottonwoods. The remainder of undeveloped floodplain is occupied by high desert sage and grasses while the developed

floodplain, immediately adjacent to the channel, is mostly used for growing alfalfa. Lahontan Reservoir is used to irrigate fields in Lahontan Valley and is managed as a warm water fishery. The reservoir also serves as a major sediment trap for the system (Miller et al., 1995).

3. The January 1997 flood

During the period from late December 1996 through early January 1997, heavy rains on a pre-existing snow-pack resulted in the largest recorded downstream flood for the Carson River. Fig. 2 provides the annual peak discharge from 1911 to 1998 and shows that the highest recorded discharge at the FCH gage occurred during the 1997 flood with an estimated (the gage was lost during the event) mean daily flow of 630 m^3/s (22,300 ft^3/s). For comparison, the designated 100-year event occurred in 1986 with a peak discharge of 470 m^3/s (16,600 ft^3/s).

3.1. Geomorphic survey of 1997-flood effects

Miller et al. (1999) conducted an extensive survey of the Carson River in the early spring following the 1997 flood. The objective was to quantify the transport and storage of trace metals and sediment within the Carson River Valley during a rare-magnitude event. Both bank erosion and overbank deposition were evaluated using geomorphic techniques of aerial photography and floodplain mapping. Data was discretized into 10 river reaches defined by valley slope and floodplain width. A description of each reach is presented in Table 1. Below is a summary of field methods and subsequent data collected during the 1997 geomorphic survey of the Carson River. For a complete discussion on techniques and results, see Miller et al. (1999).

3.1.1. Observed bank erosion

The erosional effects of the 1997 flood were dramatic. Miller et al. (1999) documents the removal of bridge embankments and approach ramps, damage to irrigation facilities, local removal of fence lines constructed along the pre-flood channel, destruction of the FCH gaging station previously located on the valley floor well beyond the channel margins, localized erosion of man-made levees constructed for flood control and the abundance of riparian trees with exposed root structures previously covered. Total bank erosion was measured by comparing aerial photographs taken in 1991 and 1997. Using the photographs, the river was discretized into 65, 1-km segments between Deer Run Road (DRR) and the river's delta. Miller et al. (1999) observed that the average change in channel width between 1991 and 1997 was 30 m, with over 80% of the sites exhibiting more than 10 m of width increase and sections

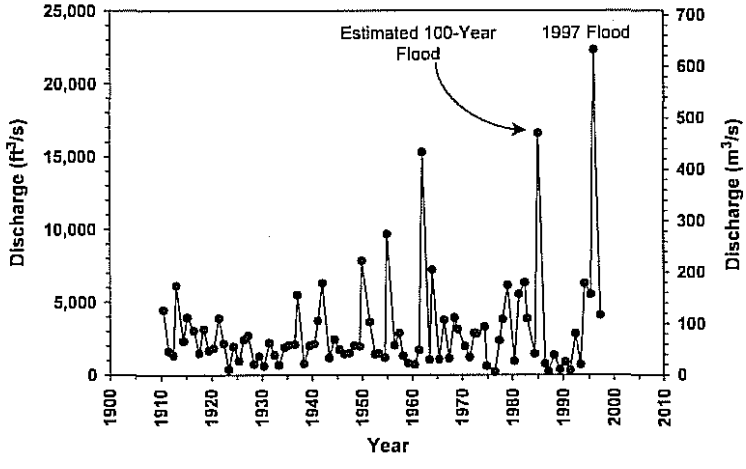

Fig. 2. Annual peak discharge at FCH from 1911 to 1998.

Table 1
Defined reach characteristics along the Carson River and correlation with modeled segments

Reach	Distance from CCG (km)	Average valley width (m)	Average slope (m/m)	Corresponding model segments
1	11.0–24.0	163	0.0043	23–48
2	24.0–27.5	354	0.0032	49–55
3	27.5–29.0	301	0.0033	56–58
4	29.0–42.5	1125	0.0014	59–85
5	42.5–47.5	460	0.0012	86–95
6	47.5–56.5	193	0.0009	96–101
7	56.5–61.0	753	0.0007	102–122
8	61.0–66.0	579	0.0007	123–132
9	66.0–70.5	831	0.0004	133–141
10	70.5–80.0	1189	0.0008	142–152

increasing up to a maximum of 280% of their pre-flood condition.

To quantify error in observed mean width changes along the Carson River, normality was assumed so that Eq. (1) could compute the 95% confidence interval in the observed mean width change per unit reach length,

$$\bar{w}^* \pm t_c \frac{S^*}{\sqrt{N-1}} \tag{1}$$

where the mean width change per unit reach length is given by,

$$\bar{w}^* = \frac{\bar{w}}{L} = \frac{\dfrac{\sum_{i=1}^{N} w_i}{N}}{L} \tag{2}$$

the standard deviation per unit reach length is given by,

$$S^* = \frac{S}{L} = \frac{\sqrt{\dfrac{\sum_{i=1}^{N} (w_i - \bar{w})^2}{N}}}{L} \tag{3}$$

where t_c is the Student's t-statistic. For this study, a two tailed test with $p = 0.05$ and $N - 1$ degrees of freedom were used. Table 2 provides reach-by-reach information on observed mean width increases and the 95% confidence interval.

3.1.2. Observed overbank deposition

Overbank deposits were defined, characterized and sampled from newly created flood deposits along the valley floor at seven locations (Miller et al., 1999). These sites were chosen to correspond with sites that were surveyed prior to the flood. Transects were positioned perpendicular to the channel with sedimentology and thickness of the overbank deposits described in pits excavated through the flood materials at regular intervals. Composite samples were collected over the entire thickness of each of the major units observed in the walls of the excavated pits. Sediments were analyzed for grain-size distribution using wet-sieving and pipeting techniques (Miller et al., 1999). Three separate overbank units were subsequently mapped.

The first delineated unit was predominantly coarse material deposited within the cottonwood and tall shrub (1–2 m high) adjacent to the main channel. This unit was composed mostly of medium to coarse

Table 2
Reach-by-reach information for computing 95% confidence interval about the observed mean width increase per unit reach length

Reach	L (km)	n	$\bar{w}$ (m)	$\bar{w}^*$ (m/km)	t_c, $p = 0.05$	S^* (m/km)	95% CI	
							Lower (m/km)	Upper (m/km)
1	12.50	14	19.16	1.53	2.16	1.26	0.78	2.29
2	3.00	3	16.20	5.40	4.30	5.28	−10.66	21.45
3	1.00	2	9.24	9.24	12.71	2.06	−16.92	35.40
4	13.00	14	29.51	2.27	2.16	0.30	2.09	2.45
5	4.50	5	27.14	6.03	2.78	1.18	4.40	7.66
6	2.50	4	45.14	18.06	3.18	2.25	13.93	22.18
7	10.00	11	31.79	3.18	2.23	0.38	2.91	3.44
8	4.50	5	21.38	4.75	2.78	1.23	3.04	6.45
9	4.00	2	57.85	14.46	12.71	0.74	5.04	23.87
10	3.00	4	44.52	14.84	3.18	1.78	11.56	18.11

sand with less than 5% silt and clay. However, the deposit did exhibit lamininae of fine-grained material in areas adjacent to the channel where man-made levees had been constructed to prevent overbank flooding. Generally, the distribution of the unit was controlled by woody vegetation. The vegetation (and consequently the deposit) were commonly confined to within 50 m of the channel banks. To compare with model results, the grain-size distribution was determined to be approximately 11% washload ($d < 0.063$ mm) and 89% coarse material ($d > 0.063$ mm). The thickness of this unit was highly variable with depths ranging from 0.1 m to greater than 2.0 m.

The second delineated unit was also comprised of mostly coarse material (11% washload, 89% coarse material). The course deposits were predominantly fine to medium sand with the quantity of fine material increasing with distance from the bank margins. This unit tended to occur within tens of meters of the channel banks. It was most extensive in reaches with wide valley floors with large, open, agricultural fields, and is absent from reaches 1, 3 and 9. Depth of deposition ranged from 0 to 45 cm (average 30 cm).

The third, and final, delineated unit was also deposited on open and/or agricultural land. However, this unit contained more fine-grained material of silt and clay. To compare with modeling results, this unit was estimated at approximately 44% washload and 56% coarse material. It was the least extensive of the three units surveyed, tended to be relatively thin (0–20 cm thick) and generally was found at greater distances from the channel margins than either of the coarse-grained overbank units. Often this unit was difficult to delineate because the material had incompletely buried grasses, and other low-lying vegetation, growing on the pre-flood valley floor.

The areal extent of the overbank deposits along the entire river was determined by matching and extrapolating field delineated units to corresponding units on 1997 aerial photographs. Data were then transferred onto USGS 7.5 min topographic maps using a vertical sketchmaster and quantified with a digital planimeter. A summary of overbank deposits is given in Table 3.

Table 3
A summary of reach-by-reach data pertaining to the three delineated units of overbank deposition

	Reach									
	1	2	3	4	5	6	7	8	9	10
Unit 1: Vegetated										
Area (km^2)	0.17	0.22	0.02	1.41	0.08	0.25	1.52	0.39	0.04	0.53
Min (cm)	25	25	25	25	25	25	25	25	25	25
Avg. (cm)	50	50	50	50	50	50	50	50	50	50
Max (cm)	75	75	75	75	75	75	75	75	75	75
Density (g/cm^3)	1.6	1.6	1.6	1.6	1.6	1.6	1.6	1.6	1.6	1.6
Unit 2: Overbank sand										
Area (km^2)	0.00	0.24	0.00	1.20	0.36	0.05	1.80	0.03	0.00	0.28
Min (cm)	5	5	5	5	5	5	5	5	5	5
Avg. (cm)	10	10	10	10	10	10	10	10	10	10
Max (cm)	30	30	30	30	30	30	30	30	30	30
Density (g/cm^3)	1.6	1.6	1.6	1.6	1.6	1.6	1.6	1.6	1.6	1.6
Unit 3: Overbank fines										
Area (km^2)	0.00	0.14	0.00	0.70	0.16	0.30	0.91	0.07	0.00	0.89
Min (cm)	2	2	2	2	2	2	2	2	2	2
Avg. (cm)	5	5	5	5	5	5	5	5	5	5
Max (cm)	10	10	10	10	10	10	10	10	10	10
Density (g/cm^3)	1.45	1.45	1.45	1.45	1.45	1.45	1.45	1.45	1.45	1.45
Total area (km^3)	0.17	0.59	0.02	3.31	0.60	0.61	4.24	0.49	0.04	1.70

4. Modeling procedures

4.1. Model description

The numerical model of the Carson River system is divided into 273 segments starting at the Carson City gage (CCG) and continuing into Lahontan Reservoir. Most of the segments are 0.5 km in length, although some segments in the transition region between the river and reservoir were made 0.25 km to improve numeric stability. The segments corresponding to the 10 reaches where erosion and overbank deposition were measured are shown in the last column of Table 1. Miller et al. (1999) compared channel width changes from aerial photos taken 2/12/91 and 2/14/97. Therefore, to compare modeled width changes to observed values, it was necessary to model mean daily discharges over this entire time span and not just during the peak of the 1997 flood. Fig. 3 shows the modeled hydrograph.

Two computer models (RIVMOD and WASP5) were used to simulate the transport of sediment in the Carson River. These models were originally chosen, linked and modified by Warwick and Heim (1995) with further modification by Carroll et al. (2000). While an attempt is made to clarify model parameterization done in terms of overbank process of erosion and deposition, one is encouraged to refer to Warwick and Heim (1995), Heim and Warwick (1997), Carroll et al. (2000), and Carroll and Warwick (2001) for a complete discussion on model development prior to this study.

RIVMOD (Hosseinipour and Martin, 1990) is a US EPA one-dimensional hydrodynamic routine that simultaneously solves standard fluid equations of continuity and momentum. Finite difference equations are solved by the Newton–Raphson method to determine flow velocity and depth given unsteady flow conditions. Early alterations to RIVMOD include a revision of the simple rectangular channel geometry to a more complex shape (Warwick and Heim, 1995). Fig. 4 shows the modified cross-sectional geometry, the associated RIVMOD parameters and parameter dimensions for the FCH site (segment 140). RIVMOD input requires bed elevation, channel roughness (Manning's n), water viscosity, channel cross-sections and initial conditions of discharge and water depth. Boundary conditions of discharge are also necessary and all input is specified in English units.

WASP5 (Ambrose et al., 1991) is the US EPA Water Quality Analysis Simulation Program-5 that was developed to simulate the transport and transformation of various water body constituents. Mass balance equations account for all material entering and leaving model segments through direct and diffuse loading, advective and dispersive transport, and any physical or chemical transformation. Input parameters required by WASP5 are given in SI units and include simulation and output control, model segmentation, advective and dispersive transport

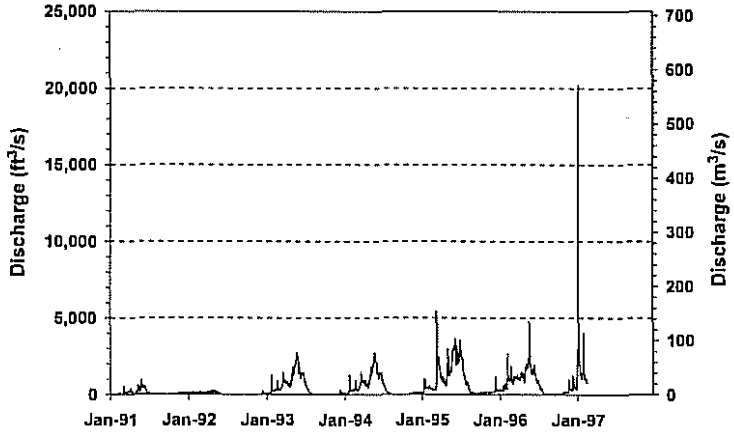

Fig. 3. Model hydrograph to simulate bank erosion from 1991 to 1997 flood (hydrograph corresponds to dates of aerial photographs).

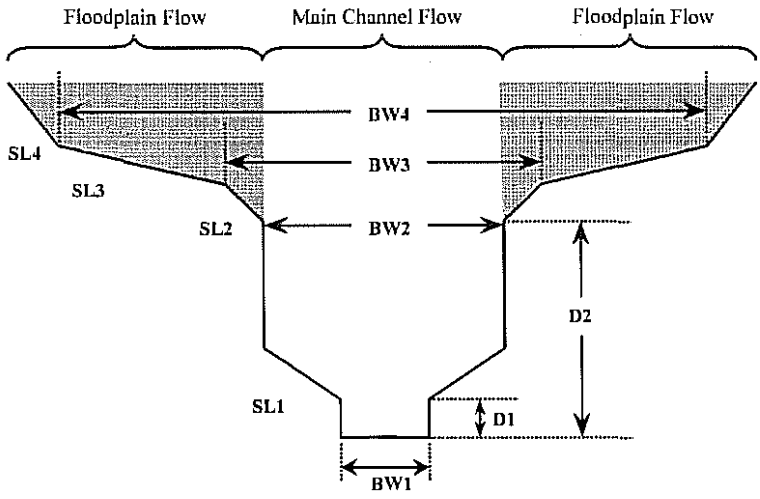

Fig. 4. Modeled cross-sectional geometry with FCH (segment 140) parameters provided. Regions of the main channel and floodplain are shown.

variables, boundary concentrations, point and diffuse source loads, and finally initial conditions. The original version of WASP5 did not simulate sediment transport, only net settling of particles. Modifications to the code include the use of measured rating curves to model the movement of solids (Carroll et al., 2000; Heim and Warwick, 1997).

4.2. Modifications to RIVMOD

Past research along the Carson River considered cross-sectional geometry spatially variable but temporally fixed (Carroll et al., 2000). In this study, modifications were made to the RIVMOD code to allow dynamic width adjustment. During every time-step, the modeled mass eroded was used to update channel width (BW2 in Fig. 4) by assuming the entire vertical face of the bank is susceptible to erosion. This implies that, on average, a 1-m width increase will produce 2.0 m^2 of sediment (which is multiplied by the segment length to get volume). Mass and volume are interchangeable by assuming a bulk density of 2.65×10^3 kg/m^3.

In order to model sediment transport during overbank discharge it is necessary to calculate the depths and velocities of flow that occur on the floodplain. The previous version of RIVMOD (Warwick and Heim, 1995) assumed a constant velocity across the entire channel profile. This assumption is no longer valid if flows in the main channel and floodplain are assumed to have different depths and hydraulic characteristics. The divided channel approach, as presented by Henderson (1966), is a classic approach to vary velocity across the channel while maintaining a constant pressure head (i.e. horizontal profile in the lateral direction). This is accomplished by assuming the true mean velocity head is obtained by weighting the area of flow with each segmented region. Specifically, RIVMOD was re-coded to consider two segmented regions of flow. The first region pertains to flow within, and directly above, the confines of the main channel while the second region accounts for flow on the floodplain (see Fig. 4). Modifications were made to estimate the cross-sectional areas, hydraulic radii and top widths for each of these regions.

Similarly, derivatives with respect to depth were calculated for each of these parameters. Further modification was made to the structure of the input file to allow the user to specify a separate floodplain Manning's roughness coefficient for each modeled segment.

Given that these modifications to RIVMOD already directly consider the segmented areas of flow in its computation of mean discharge it was not necessary to correct the continuity equation. However, a velocity correction coefficient for the momentum equation (α) was necessary. The derivation of α is provided in Eq. (4) with A being the cross-sectional area and K the conveyance. The subscript (i) refers to each segmented region across the channel profile (i.e. 1 = main channel, 2 = floodplain).

$$\alpha = \frac{\sum_{i=1}^{2} A_i}{\left(\sum_{i=1}^{2} K_i\right)^2}\left[\sum_{i=1}^{2} (K_i^2/A_i)\right] \tag{4}$$

The conveyance K provides a convenient method for equating the friction slopes of each region, as is shown with Eq. (5). Here, Q is the flow and S_f is the friction slope.

$$\frac{Q_1}{K_1} = \frac{Q_2}{K_2} = \frac{\sum_{i=1}^{2} Q_i}{\sum_{i=1}^{2} K_i} = S_f^{0.5} \tag{5}$$

Using Eq. (5) and Manning's equation, it is possible to solve for each region's conveyance with Eq. (6), given R is the hydraulic radius.

$$K_i = 1.486 A_i R_i^{2/3} \tag{6}$$

RIVMODs momentum equation, as presented by Warwick and Heim (1995), is shown with Eq. (7).

$$R_2 = \frac{\partial x}{g A_m}\left(\frac{\partial Q_m}{\partial t}\right) + \frac{\partial x}{g A_m}\left[\frac{\partial}{\partial x}\left(\frac{Q_m^2}{A_m}\right)\right] + \frac{\partial x q v}{g A_m} + \partial x(s_f - S_0) \tag{7}$$

Here, x (ft) is distance in the downstream direction, g (ft/s^2) is the acceleration due to gravity, A_m (ft^2) is the mean cross-sectional area between the upstream and downstream stations, Q_m (ft^3) is the mean discharge between the upstream and downstream stations, t is time (s), q is lateral inflow (ft^2/s), v (ft/s) is velocity, S_f is the friction slope, S_0 is the channel bottom slope and R_2 is the momentum residual.

Subsequent modifications to Eq. (7) include using Eq. (5) to calculate S_f as well as the addition of the momentum correction factor (α) to the second term. The later of these modifications is shown with Eq. (8). Note that α is not placed within the partial derivative. While α is a function of depth and flow, it is assumed that α is not a function of small changes in x.

$$Q = \frac{\partial x \alpha_m}{g A_m}\left[\frac{\partial}{\partial x}\left(\frac{Q_m^2}{A_m}\right)\right] \tag{8}$$

A simple 7-segment model was used for to validate RIVMOD code modifications. Uniform cross-sections, a constant longitudinal slope and floodplain roughness coefficients set equal to the main channel roughness coefficients were used. First, numeric dispersion was checked by reducing the model's segment spacing (Δx) and time-step (Δt), independently. Resulting flow depths (segment 2), given steady state simulations of 142, 283, 425, 566, 708 and 850 m^3/s, are listed in Table 4 and illustrate that numeric dispersion is not

Table 4
Validation of the modified RIVMOD code for steady state simulations

Discharge (ft^3/s)	Discharge (m^3/s)	Modified RIVMOD			Previous RIVMOD	HEC-RAS
		$\Delta t = 5$ s; $\Delta x = 0.402$ km	$\Delta t = 5$ s; $\Delta x = 0.201$ km	$\Delta t = 1$ s; $\Delta x = 0.402$ km		
5000	142	2.83	2.83	2.83	2.83	2.84
10,000	283	3.74	3.74	3.74	3.74	3.73
15,000	425	4.44	4.44	4.44	5.12	4.45
20,000	566	4.81	4.81	4.81	5.24	4.80
25,000	708	5.02	5.02	5.02	5.37	4.94
30,000	850	5.17	5.17	5.17	5.47	5.19

impacting the modified version of RIVMOD. Also included in Table 4 are the steady state results from the previous version of RIVMOD and the well-established HEC-RAS (Brunner et al., 1998). HEC-RAS is a public domain model distributed by the US Army Corp of Engineers. It is capable of computing one-dimensional water surface profiles for steady gradually varied flow. Results show that the previous version and newly modified versions of RIVMOD do not predict equivalent depths when flows surpass bankfull discharge (for the 7-segment model this occurs at flows larger than 283 m^3/s). Instead, the former version gives substantially greater depths. On the other hand, there is excellent agreement between the modified RIVMOD and HEC-RAS.

Using the same simple 7-segment model, validation was also accomplished by comparing unsteady flow results between both versions of RIVMOD and HEC-UNET (Barkau, 1997). HEC-UNET is an unsteady flow model developed by the US Army Corp of Engineers. It solves unsteady flow equations of continuity and momentum in one-dimension using an implicit finite difference scheme (four point implicit, or box, scheme). An initial flow of 14.2 m^3/s (500 ft^3/s) was run for 3 days to ensure steady conditions. After steady conditions were obtained, a 40-day symmetric hydrograph was simulated (see Fig. 5a). Results (segment 2) are shown in Fig. 5b. The previous version of RIVMOD appears unstable when flows initially break out onto

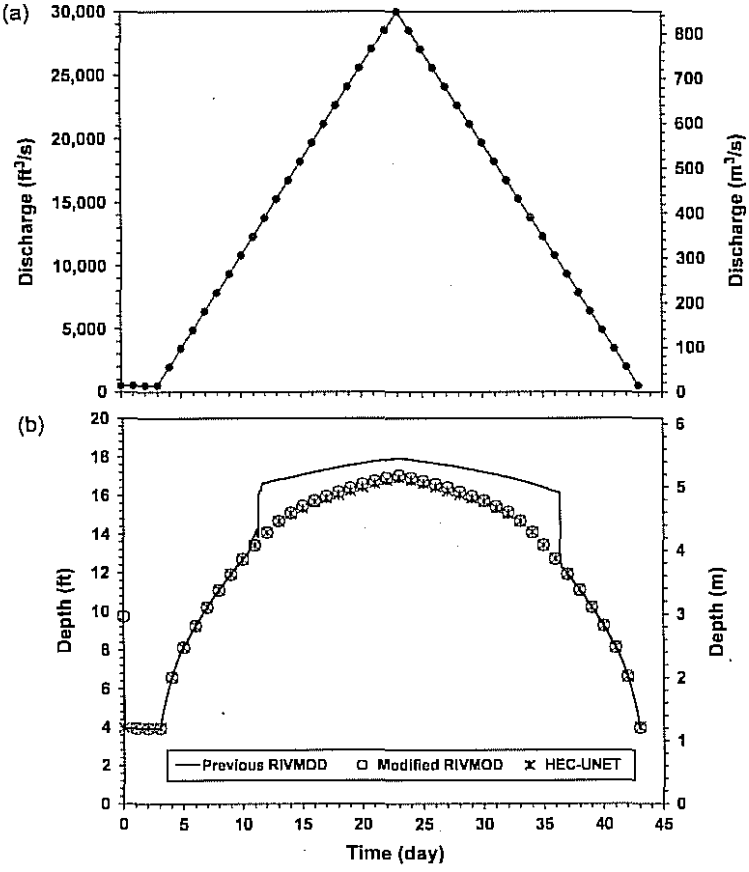

Fig. 5. Validation of the RIVMOD code for unsteady flow conditions: (a) modeled hydrograph, (b) depth comparisons between the previous version of RIVMOD, the modified version of RIVMOD and the US Army Corp of Engineer's accepted model HEC-UNIT.

the floodplain, and again predicts greater flow depths above bankfull discharge than its modified counterpart. On the other hand, the modified version of RIVMOD and HEC-UNET estimate nearly equivalent depths at all flows.

Validation of the newly modified RIVMOD shows the model is successful in simulating flows greater than bankfull discharge. Instabilities are eliminated when flows first breakout onto the floodplain and depths match other accepted hydrodynamic models. The modified version of RIVMOD also provides greater flexibility for the user by allowing separate floodplain roughness coefficients. In this study, all simulations of the Carson River maintain channel roughness coefficients ($n = 0.035–0.045$) used in previous studies (Carroll et al., 2000; Heim and Warwick, 1997; Warwick and Heim, 1995), but incorporate a floodplain roughness coefficient of 0.100 for all model segments. The value of 0.100 falls in the range of roughness coefficients presented in the literature for winding, weedy, overgrown and/or debris filled regions (Dudley et al., 1998; Henderson, 1966).

4.3. Modeling sediment transport

WASP5 is capable of modeling three distinct solid types. Washload constitutes the smallest fraction ($d < 0.063$ mm) and is considered uniformly distributed from the riverbed to the water's surface. Data from Katzer and Bennett (1983) indicates that approximately 30% of the washload is colloidal ($d < 0.002$ mm) which is assumed to always remain in suspension. Coarse suspended sediment (CSS) is larger ($d > 0.063$ mm) and its concentrations in the water column are greatest near the riverbed and diminish upward toward the water surface. This is a direct reflection of the exchange of bed material into suspension and vice versa Meade (1990). Bedload is the third type of solid modeled. It is defined as the coarse material that travels by rolling, skipping and/or sliding along the river bed.

Rating curves, fit to USGS water column data collected at CCG, for washload ($r^2 = 0.77$) and CSS ($r^2 = 0.99$) were written directly into the WASP5 code as upstream boundary conditions (Carroll et al., 2000). USGS data collected near the river's downstream boundary (FCH) showed a net increase of washload, when compared to CCG for any given discharge. Observed data (Miller et al., 1998) suggests approximately 30% of the bank material is washload. It is assumed that bank erosion is the source of additional washload in the water column at FCH, and subsequent calibration of the bank erosion function, given flows below bankfull discharge, reflects this assumption (see Section 4.4, Eq. (12)). At flows surpassing bankfull discharge, washload entering the system, via bank erosion, may either remain in the water column to be transported downstream, or it may be deposited on the floodplain. Subsequently, the function describing washload overbank deposition (see Section 4.5, Eq. (19)) is calibrated to best match washload concentrations in the channel at FCH during overbank flows.

While 30% of the eroded bank material is fine, the other 70% is coarse. However, data suggests that CSS is held constant, for any given flow, between CCG and FCH ($r^2 = 0.86$). Modeled concentrations of CSS and bedload must accommodate the addition of this coarse material added from bank erosion. When flows are contained within the confines of the main channel it is assumed that any CSS eroded above and beyond that needed to satisfy the USGS rating curve at FCH settles onto the bed segment and is transported as bedload. However, when flows surpass bankfull discharge, eroded coarse material becomes a source for overbank deposition. Coarse material that is not deposited on the floodplain is deposited on the bed segment and transported as bedload.

No data for bedload exists along the Carson River. To model bedload, the bedload transport rate q_b (kg/s) was assigned the following upstream boundary condition,

$$q_b = aQ_{main}^2 \tag{9}$$

where Q_{main} (m^3/s) is the discharge within, and directly above, the main channel and the a-coefficient (kg s/m^6) is a calibration parameter. This rating curve was chosen primarily for its simplicity and to mimic the rating curves used to define the upstream boundary conditions for washload and CSS. The a-coefficient in Eq. (9) was adjusted to match long-term average annual sedimentation loads into Lahontan Reservoir. The average annual sediment load into the reservoir was approximated at 404,000 tons/year by Miller et al.

(1995). Estimates were established by measuring thickness, extent and bulk density of deposited material at several locations within the reservoir when reservoir stage was extremely low. About 90% of this total (363,000 tons/year) is believed to be a direct result of loading from the Carson River while the remaining 10% is assumed to be derived from lateral erosion of the reservoir, sediment from the Truckee Canal and eolian transport (Heim and Warwick, 1997; Miller, personal communication). Results of modeled sedimentation into Lahontan Reservoir are provided in Table 5. Mean daily flows at the FCH gage from 1911 (construction of Lahontan Reservoir) to 1992 (year of sediment survey) were divided into 10 categories, averaged and run in the model at steady state. Loads for each flow regime were weighted by the number of days of occurrence (excluding zero flows since these transport no mass). The a-coefficient was adjusted to 0.0145 so that bedload, when added to CSS and non-colloidal washload, matched the target value of 363,000 tons/year. Model results suggest that large flows ($>100\ m^3/s$), which occur less than 0.5% of the time from 1911 to 1992 (given all non-zero flows), may transport more about 22% of the material into the reservoir. Results also show that more frequent moderate flows ($20–60\ m^3/s$) may be responsible for more than 50% of the material deposited in the reservoir.

4.4. Modeling bank erosion

To model bank erosion, it was assumed that the lateral erosion rate, LE (m/s) is proportional to the shear stress applied to the bank, τ_{bank} (kg/m per s^2) (Darby and Thorne, 1996). It is also assumed that LE is indirectly related to the average velocity, or square-root of the channel bottom slope as defined by Manning's equation, such that,

$$LE \propto \frac{\tau_{bank}}{S_0^{0.5}} \tag{10}$$

As with Carroll et al. (2000), Eq. (10) implicitly assumes the river is in vertical equilibrium with erosion and/or deposition occurring laterally across the floodplain and not along the channel bed (Miller, personal communication). Eq. (10) also implies that reaches with steep longitudinal slopes (higher stream power) have already displaced much of their fine material from the channel banks. Conversely, portions of the river that dip only slightly still contain a large proportion of their fine sediment in the channel banks and may experience more lateral erosion. Fig. 6 shows the longitudinal slopes of the Carson River with reaches 1–10 marked. The steeper reaches have essentially 'blown out' much of their fine material and contain mostly cobble and pebble size particles. Lateral erosion is further inhibited by bedrock canyon walls (Miller et al., 1998). On the other hand,

Table 5
Calibration results for bedload transport by matching 81-year average annual sedimentation into Lahontan Reservoir

Flow range (ft^3/s)	Average flow		# Days occurring in record	Mass deposited in reservoir			
	ft^3/s	m^3/s		Non-colloidal WL (tons/year)	CSS (tons/year)	Bedload (tons/year)	Total (tons/year)
≥10,000	11,633	329	3	1219	1438	9436	12,093
4000–10,000	5400	153	57	3337	5893	40,398	49,628
3500–4000	3699	105	47	625	2281	16,268	19,174
3000–3500	3229	91	98	3506	3624	18,979	26,110
2500–3000	2705	77	147	3830	3816	19,767	27,413
2000–2500	2213	63	341	6145	5925	31,334	43,404
1500–2000	1720	49	720	8201	7554	41,140	56,894
1000–1500	1213	34	1488	9056	7768	44,350	61,175
500–1000	704	20	3296	7666	5796	36,081	49,544
<500	167	5	19,112	2970	1895	13,309	18,174
0	0	0	3161	0	0	0	0
			Total (tons/year)	46,556	45,990	271,063	363,609

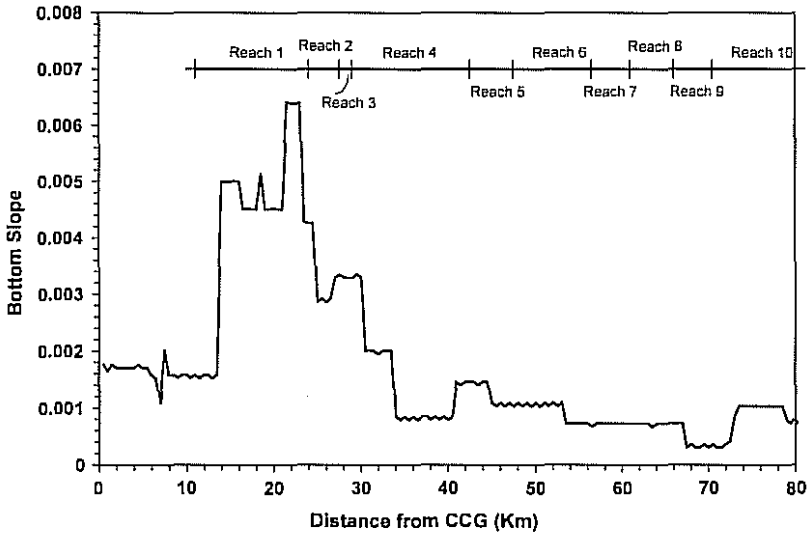

Fig. 6. Measured longitudinal bottom slopes along the Carson River with reaches 1–10 marked.

the downstream reaches contain wider valleys dominated by fines and the river exhibits a typical meandering pattern. This conceptual model of bank erosion is verified by fieldwork conducted by Miller et al. (1999) who discovered a statistically significant inverse correlation between a change in channel width (bank erosion) and channel slope (correlation analysis produces $p = 0.05$, $r = 0.66$).

Shear stress applied to the bank is assumed correlated to the average shear stress applied to the channel perimeter, such that,

$$\tau_{\text{bank}} = \gamma_w D S_f \tag{11}$$

where γ_w is the specific weight of water (kg/m^2 per s^2), D is the water depth starting at the vertical face of the channel bank (m), and S_f is the friction slope. Using Manning's equation (assuming the channel is wide) gives the following,

$$\text{MER} = \frac{\psi_1 \rho_s \gamma_w n^2 D^{2/3} v^2 L_s}{S_0^{1/2}} \tag{12}$$

where v is the water velocity (m/s), n is Manning's coefficient, L_s is the segment length (m), and ψ_1 is a constant of proportionality (m^2 s/kg). ψ_1 is calibrated using measured water column concentrations of washload material at FCH. Reasons for calibration are described in Section 4.3.

To model erosion during overbank flows the same function is kept for the portion of flow within bank, but a second term was added to account for the underlying change of character as the river exceeds bankfull flow (Ervine et al., 2000) where h is the height of the vertical bank face (see Fig. 4).

$$\text{MER}_{\text{OB}} = \frac{\psi_1 \rho_s \gamma_w n^2 D^{2/3} v^2 L_s}{S_0^{1/2}} + \frac{\psi_2 \rho_s \gamma_w n^2 (D-h) v^2 L_s}{h^{1/3} S_0^{1/2}} \tag{13}$$

The constant ψ_2 (dimensionally equivalent to ψ_1) is calibrated so that the total modeled mass eroded from the banks falls within the range presented by Miller et al. (1999).

4.5. Modeling overbank deposition

Washload and CSS overbank deposition are modeled separately along the Carson River. To model CSS deposition on the floodplain, the water above the floodplain is assumed to be completely mixed and interacting with a single layer of sediment such that, for steady state conditions, the rate of sedimentation R_s (kg/s per m^2) is given by

(Thomann and Mueller, 1987),

$$R_s = V_s C \tag{14}$$

where V_s is the average particle settling velocity (m/s) and C is the concentration of solids in the water column (kg/m^3).

It is assumed that deposition of CSS will diminish exponentially away from the main channel (Walling and He, 1997; Mount, 1995), such that,

$$C^c_{flood} = C^c_{main}\, e^{-X_f/\kappa} \tag{15}$$

where X_f is the lateral distance from the edge of the main channel across the floodplain and κ is a constant that represents the general decline in CSS with distance from the main channel. Walling and He (1997) estimate an average value for κ of 15. C^c_{flood} and C^c_{main} are CSS water column concentrations (kg/m^3) in the floodplain and main channel, respectively. To determine the rate of sedimentation, C^c_{flood} is substituted into Eq. (14) for the water column concentration C and integrated with respect to X_f. The rate of CSS deposition (R^c_s) is subsequently estimated using Eq. (16).

$$R^c_s = \kappa V^c_s C^c_{main}(1 - e^{-X_f/\kappa}) \tag{16}$$

Values of X_f, and C^c_{main} are provided by RIVMOD and WASP5. Early modeling efforts of the Carson River have established an average CSS diameter equal to 0.13 mm, with an upper limit of 0.20 mm (Carroll et al., 2000). Using Stokes' relation to calculate the settling velocity of an average sized CSS particle gives a value for V^c_s of 0.015 m/s.

Deposition of washload material on the floodplain during overbank events is modeled using a method for determining the rate of deposition of sediment in the model WEPP (Foster et al., 1995). The rate of washload deposition R^w_s (kg/s per m^2) is given by

$$R^w_s = \frac{\bar{\beta} V^w_s}{q_f}(G^w_{main} - T_c) \tag{17}$$

where V^w_s is the average fall velocity for washload material (m/s) and q_f (m^2/s) is the discharge per unit width on the floodplain. Using Stoke's law and assuming an average washload particle diameter of 0.033 mm (non-colloidal washload 0.002–0.63 mm), V^w_s equals 0.001 m/s. G^w_{main} is the water column non-colloidal washload (kg/s per m) in the main channel and T_c is the transport capacity (kg/m per s). Eq. (17) predicts that sediment will be eroded if the transport capacity exceeds G^w_{main}, however, the current modeling approach does not allow erosion to occur on the floodplain (i.e. $G^w_{main} \geq T_c$). β is a dimensionless turbulence coefficient and is assumed to decay exponentially such that $\beta = 0$ when $X_f = 0$ and $\beta = 0.5$ when $X_f = 2.0$ m. The average β across the floodplain is consequently defined as,

$$\bar{\beta} = \int_0^{X_f} (1 - e^{-0.347x})dx = 1 - \frac{(1 - e^{-0.347X_f})}{0.347X_f} \tag{18}$$

To estimate T_c, a modified form of the model applied by Johnson et al. (2000) is used:

$$T_c = \psi_3 q^2 S_0^{1.66} \tag{19}$$

where ψ_3 is a calibration constant (kg s/m^5) adjusted match washload water column concentrations at FCH during overbank flows.

5. Results

5.1. Erosion

Table 6 provides a list of calibration parameters, their relevant equations, final values and objectives matched in the calibration process. Using $\rho_s = 2.65 \times 10^3$ kg/m^3, $\gamma_w = 9.81 \times 10^3$ kg/m^2 per s, and an average Manning roughness value of 0.045, channel bank erosion during in-bank flows is calibrated by adjusting ψ_1 in Eq. (12) to a value of 246 m^2 s/kg to match washload water column concentrations at FCH during in-bank flows (see Fig. 7). Channel bank erosion during overbank flows is calibrated by adjusting ψ_2 in Eq. (13) to a value of 131,000 m^2 s/kg so that the predicted value of total eroded mass (or total width eroded) falls within the range of observed established by Miller et al. (1999). Calibrated values of ψ_1 and ψ_2 indicate an increase in relative amounts of mass eroded when flows go above bankfull, however, this increase is not an increase by three-orders of magnitude. A review of Eq. (13) shows that while ψ_1 is directly related to water depth (D), ψ_2 is directly related to the smaller value of depth above bankfull ($D - h$). As an example, for a flow that is slightly above overbank at FCH (99 m^3/s),

Table 6
Calibration parameters and associated values used in the model

Parameter	Equation number	Value	Units	Purpose	Objective to match
a	(9)	0.0145	kg s/m^6	Bedload transport rate upstream boundary	Long-term deposition into Lahontan Reservoir
ψ_1	(12)	246	m^2 s/kg	Bank erosion	Washload at FCH gage during in-bank flows
ψ_2	(13)	131,000	m^2 s/kg	Bank erosion	Total mass eroded between 1991 and 1997
ψ_3	(18)	2.0×10^6	kg s/m^5	Floodplain washload deposition	Washload at FCH gage during overbank flows

the percent of MER due to the first term (ψ_1) in Eq. (13) is 7%, with the second term (ψ_2) accounting for the remainder. An increase in MER when flows go overbank may be justified when one considers that flows above bankfull may be dominated by secondary flow formation, horizontal shear and the bulk exchange of fluid between the floodplain and the main channel (Ervine et al., 2000).

Total model mass eroded is compared to observed values in Fig. 8, as well as modeled mass estimates for each year of the simulation. Modeled results show that the single, catastrophic event of 1997 eroded nearly 87% of the total modeled mass. In contrast, model results for 1995 and 1996, with sustained medium-to-high flows, eroded only 8 and 4% of the total mass, respectively. The remaining lower flow years (1991–1994) constitute just 1% of the eroded mass.

No attempt was made to match reach-by-reach width increases with the calibration of ψ_1 or ψ_2. Therefore, comparing reach-by-reach width increases with observed values acts as an independent verification of the bank erosion model. Results (Fig. 9) show modeled width increases fall within the 95% confidence interval of the observed mean in seven of the ten reaches. Note that reaches 2 and 3 have large uncertainty associated with their observed means such

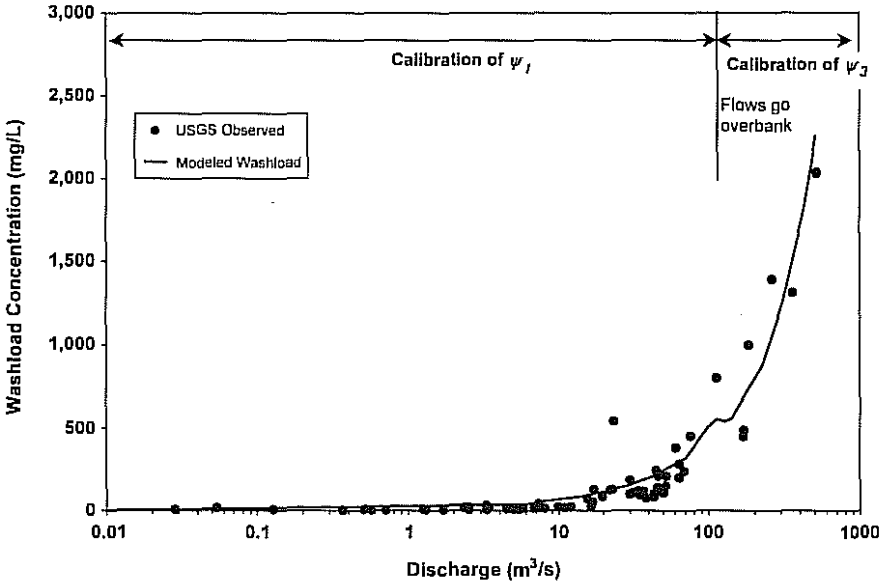

Fig. 7. Calibration of ψ_1 and ψ_3 to best match washload water column concentrations at the FCH gage.

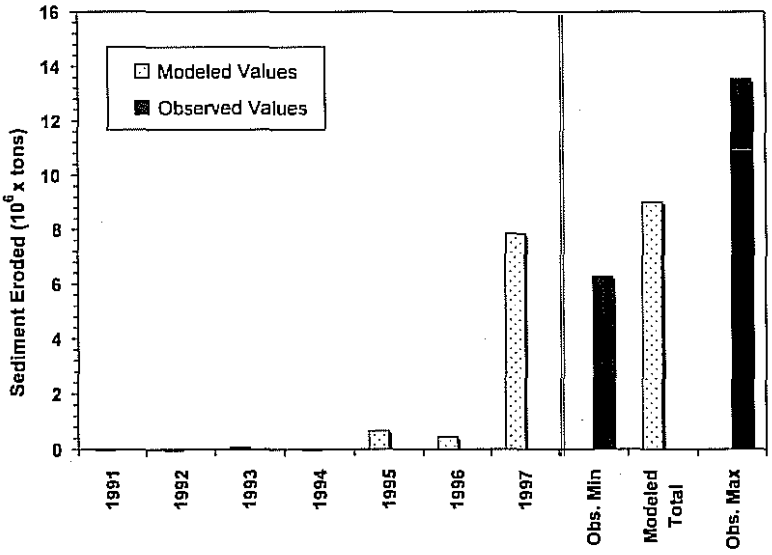

Fig. 8. Calibration of ψ_2 by matching the total observed mass eroded from 1991 to 1997.

that their 95% confidence intervals actually span negative values to imply channel narrowing. Large uncertainty is due to a large standard deviation in width measurements coupled with a small number of samples (i.e. large t_c). It is particularly encouraging, that those reaches with little uncertainty in the observed mean (reaches 1, 4, 5 and 7) are well predicted by the model. It is also encouraging that while the model is not able to predict width increase within the 95% confidence interval for reaches 6 and 8

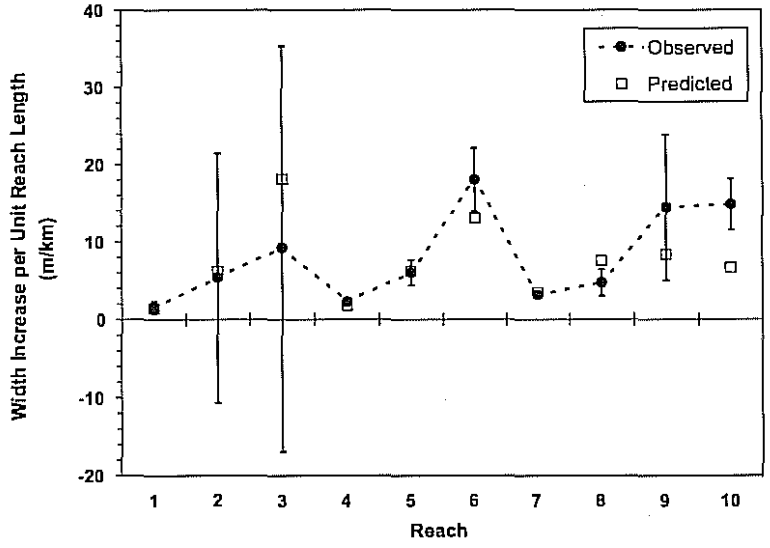

Fig. 9. Verification of the bank erosion model showing observed versus predicted width increase per kilometer on a reach-by-reach basis. Boxes indicate 95% confidence interval about the observed mean.

that the model is able to mimic the observed trend. More specifically, observed values suggest that relative bank erosion increases from reach 5 to 6 and from reach 7 to 8. Likewise, the model also predicts a relative increase in bank erosion at these locations and misses predicting in the 95% confidence interval by a relatively small amount (approximately 1 m). While reach 10 is observed to have very little change in width increase compared to reach 9, the model produces a slight lowering when compared to reach 9. This lowering in modeled erosion at reach 10 is expected since S_0 is shown to increase slightly in reach 10 (see Table 1 and Fig. 3) to generate less bank erosion (see Eq. (13)).

5.2. Floodplain deposition

A value of ψ_3 equal to 2.0×10^6 kg s/m^5 was obtained (i.e. calibrated) to optimize agreement between computed and predicted washload concentrations at FCH during overbank flows (see Fig. 7). In comparison, Johnson et al. (2000) use a value of 2.31×10^7 kg s/m^5 in WEPP to model deposition processes in rills. No attempt was made to match washload mass deposited on the floodplain (either total or on a reach-by-reach basis) and so comparing the modeled mass of washload deposition to observed values (Fig. 10a) acts as a verification of the approach. Only reaches 3 and 5 are modeled within the observed range. Of the remaining reaches, washload deposition is under predicted for 1, 2 and 6. However, observed values indicate that relatively little deposition occurs at these reaches when compared to reaches 4 and 7 and so the model mimics this trend. Conversely, reaches 4, 7, 8, 9 and 10 are drastically over predicted. The total modeled washload deposited is approximately 2.7 times greater than the upper range established by Miller et al. (1999). However, it is believed that observed values of washload mass are generally under-representative of the actual mass deposited because Miller et al. (1999) focused survey efforts on delineating predominantly coarse sediment units and the finer-grained units were difficult to survey (i.e. due to incompletely buried vegetation, thinning of sequence at margins of transect, etc). In this sense, it is encouraging that the model over predicts rather than under predicts washload sedimentation.

No calibration of the CSS overbank deposition model was attempted. Instead, results act as a true evaluation of the approach to define coarse sediment floodplain deposition. Modeled CSS overbank deposition on a reach-by-reach basis is compared to observed values in Fig. 10b. Results show that 5 of the 10 reaches (2, 4, 6, 7, and 10) fall within the range of observed values. The remaining reaches are over predicted. The over prediction of CSS deposition in these reaches could be attributed to a channel that is more incised than currently modeled. Detailed surveys may alleviate these model inaccuracies. Despite the over prediction in these five reaches, most reaches still follow the general trend observed by Miller et al. (1999) and the total modeled CSS deposited lies within the range observed by Miller et al. (1999).

6. Summary and conclusions

Sediment transport processes dictate the movement of mercury through the Carson River system. The Carson River rarely experiences overbank flows, however, when they do occur these flows have the potential to produce significant geomorphic change. As a result, flood generated bank erosion and overbank deposition become extremely important mechanisms for the cycling of mercury and need quantification. Data collected in response to the 1997-flood has allowed model calibration and verification of bank erosion and floodplain deposition during overbank discharge. Future investigation is needed to evaluate the effect of these processes on mercury transport.

The divided channel approach is applied to the momentum equation contained within the RIVMOD numeric code. The result is a more stable model that is capable of estimating floodplain depths and velocities during overbank flows. Increased flexibility allows the user to assign a separate floodplain roughness coefficient to each of the modeled segments. An empirical relationship based on shear stress applied to the banks is developed to describe bank erosion during overbank flows. Model calibration is accomplished by matching observed total mass eroded from 1991 to 1997. It is only possible to match observed values by allowing significantly more erosion to occur when flows surpass bankfull discharge than when

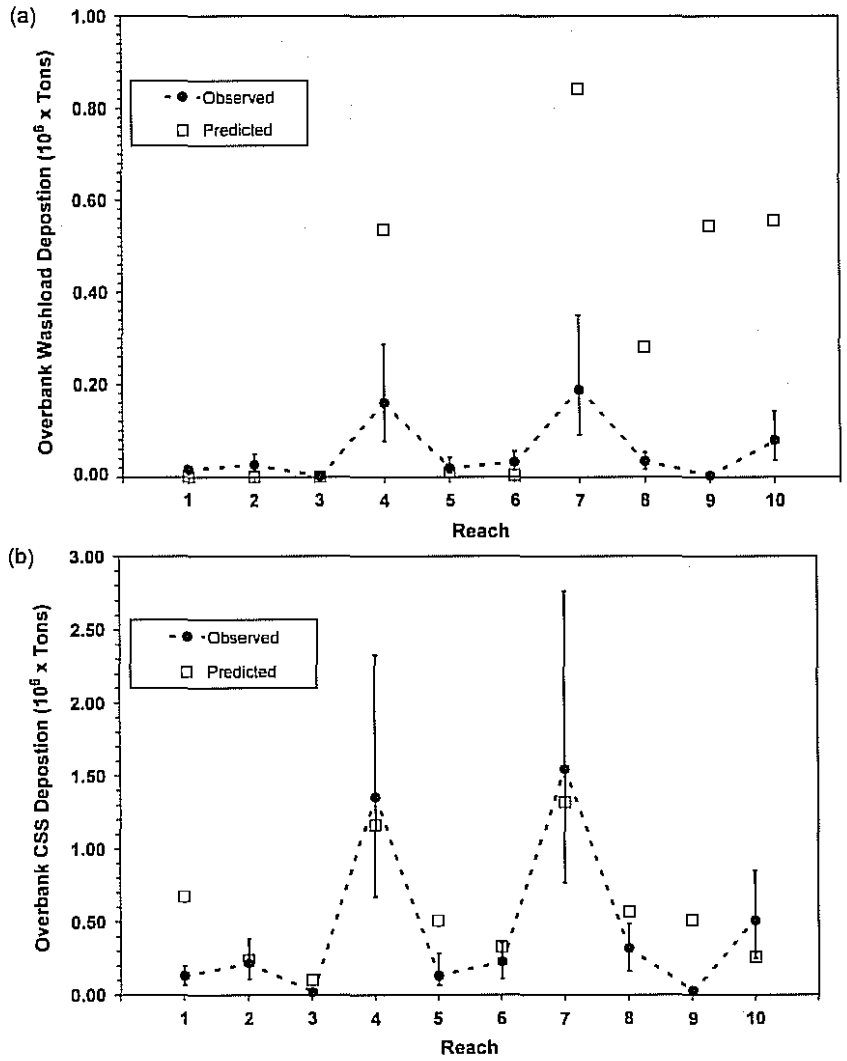

Fig. 10. Verification of the floodplain sedimentation model with a reach-by-reach comparison of modeled mass deposited on the floodplain with observed ranges. (a) Washload and (b) Coarse Material.

flows are still confined to the main channel. The result is that nearly 87% of bank mass eroded in a 6-year time span occurs during the single 1997 flood event. Model results agree with Miller et al. (1999) who attributes all geomorphic change along the Carson River from 1991–1997 to this single high-magnitude event. Verification of this approach shows the model falls within the 95% confidence interval of the observed mean channel width increase in 7 of the 10 reaches, with trends well predicted in two of the remaining three reaches.

Overbank deposition is modeled using separate, but related, approaches for CSS and washload. CSS is modeled by coupling analytical approaches presented by Thomann and Mueller (1987) and Walling and He (1997) in order to relate the amount

of sediment deposited to the distance from the main channel. With no calibration, modeled values of CSS deposition on the floodplain agree quite well with observed values by agreeing with observed values in 5 out of 10 reaches. Washload deposition is modeled using a functional relationship developed for the model WEPP that relates the rate of washload deposition to the difference between the actual concentration of sediment in the water column and the theoretical transport capacity. This function is able to predict washload concentrations at FCH, but over predicts washload deposited on the floodplain for most modeled reaches and over predicts total washload deposited by a factor of 2.7.

Acknowledgements

This study was made possible by a grant from the National Science Foundation, EAR-9712857, and a grant from the United States Environmental Protection Agency, Region IX and the US Geological Survey under cooperative agreement 00WRAG0009.

Appendix A. Notation

a	calibration parameter defining bedload transport rate q_b at CCG (kg s/m^6)
α	velocity correction coefficient for momentum (dimensionless)
α_m	mean velocity correction coefficient for momentum between an upstream and downstream station in RIVMOD (dimensionless)
A	channel cross-sectional area of a station in RIVMOD (ft^2)
A_m	mean cross sectional area between an upstream and downstream station in RIVMOD (ft^2)
$\tilde{\beta}$	average turbulence coefficient across the floodplain (dimensionless)
C^c_{flood}	concentration of coarse suspended sediment in the water column above the floodplain (kg/m^3)
C^c_{main}	concentration of coarse suspended sediment in the water column within the main channel (kg/m^3)
D	water depth starting at the vertical face of the channel bank (m)
γ_w	specific weight of water (kg/m^2 per s^2)
g	acceleration due to gravity (ft/s^2)
G^w_{main}	water column non-colloidal washload load in the main channel (kg/s per m)
h	height of vertical face of channel bank (m)
κ	constant that represents the general decline in coarse suspended sediment with distance from the main channel across the floodplain (dimensionless)
K	conveyance (subscripts 1 = main channel, 2 = floodplain)
L	reach length (km)
L_s	model segment length (m)
LE	lateral erosion rate (m/s)
MER	mass erosion rate (kg/s)
n	Manning's roughness coefficient (dimensionless)
N	number of measured cross sections (via areal photography) for calculation of observed width.
q	lateral flow rate(ft^2/s)
q_b	bedload transport rate per unit width (m^2/s)
q_f	discharge per unit width of floodplain (m^2/s)
Q_m	mean discharge between the upstream and downstream stations in RIVMOD (ft^3/s)
Q_{main}	discharge in the main channel (m^3/s)
R	hydraulic radius
R^c_s	rate of CSS deposition on the floodplain (kg/s per m^2)
R^w_s	rate of washload deposition on the floodplain (kg/s per m^2)
ρ_s	density of the bank material (kg/m^3)
R_2	momentum residual
S	standard deviation of channel width increase (km)
S^*	standard deviation of channel width increase per unit reach length (m/km)
S_0	channel bottom slope (dimensionless)
S_f	friction slope (dimensionless)
τ_{bank}	average shear stress applied to the bank (kg/m per s^2)
t	time (s)
t_c	Student's t statistic (dimensionless)
T_c	transport capacity (kg/s per m)
x	distance in the downstream direction (ft)

X_f lateral distance from the channel margin across the floodplain (m)
v velocity (ft/s in Eq. (7) and m/s in Eq. (13))
V_s^c average course suspended sediment settling velocity (m/s)
V_s^w average fall velocity for washload material (m/s)
w observed channel width increase
$\bar{w}$ mean observed channel width increase (m)
$\bar{w}^*$ mean observed channel width increase per unit reach length (m/km)
ψ_1 constant of proportionality for bank erosion below bankfull discharge (m^2(s/g))
ψ_2 constant of proportionality for bank erosion above bankfull discharge (m^2(s/g))
ψ_3 constant of proportionality for total washload deposited on the floodplain (g s/m^5)

References

Ambrose, R.B., Wool, T.A., Martin, J.P., Schanz, R.W., 1991. WASP5.X: A Hydrodynamic and Water Quality Model: Model Theory, User's Manual and Programmer's Guide, USEPA, Athens, Georgia.

ASCE Task Committee on Hydraulics, Bank Mechanics and Modeling River Width Adjustment, 1998. River width adjustment. II. Modeling. Journal of Hydraulic Engineering-ASCE 124(9), 903–917.

Barkau, R.L., 1997. UNET: One-Dimensional Unsteady Flow through a Full Network of Open Channels, US Army Corp of Hydrologic Engineering Center, Davis, CA.

Bates, P.D., Horritt, M., Hervouet, J.M., 1998. Investigating two-dimensional, finite element predictions of floodplain inundation using fractal generated topography. Hydrological Processes 12, 1257–1277.

Bonzongo, J.C., Heim, K.J., Warwick, J.J., Lyons, W.B., 1996. Mercury levels in surface waters of the Carson River–Lahontan Reservoir system, Nevada: influence of historic mining activities. Environ Pollution 92(2), 193–201.

Brunner, G.W., Jensen, M.R., Piper, S.S., Klipsch, J., Montalvo, A., Daly, S.F., Warner, J.W., 1998. HEC-RAS: River Analysis System User Manual, US Army Corp of Hydrologic Engineering Center, Davis, CA.

Carroll, R.W.H., Warwick, J.J., 2001. Uncertainty analysis of the Carson River mercury transport model. Ecological Modeling 137, 211–224.

Carroll, R.W.H., Warwick, J.J., Heim, K.J., Bonzongo, J.C., Miller, J.R., Lyons, W.B., 2000. Simulating mercury transport and fate in the Carson River, Nevada. Ecological Modeling 125, 255–278.

Darby, S.E., 1998. Modeling width adjustment in straight alluvial channels. Hydrological Processes 12, 1299–1321.

Darby, S.E., Thorne, C.R., 1996. Numerical simulation of widening and bed deformation of straight sand-bed rivers. I. Model development. Journal of Hydraulic Engineering 122(4), 184–193.

Dudley, S.J., Fischenich, J.C., Abt, S.R., 1998. Effects of woody debris entrapment on flow resistance. Journal of American Water Resources Association 34(5), 1189–1197.

Ervine, D.A., Babaeyan-Koopaei, K., Sellin, R.H.J., 2000. Two-dimensional solution for straight and meandering overbank flows. Journal of Hydraulic Engineering 126(9), 653–669.

Foster, G.R., Flanagan, D.C., Nearing, M.A., Lane, L.J., Risse, L.M., Finkner, S.C., 1995. Chapter 11: Hillslope erosion component. In: USDA-Water Erosion Prediction Project (WEPP) Technical Documentation. NSERL Report No. 10, National Soil Erosion Research Laboratory, USDA-ARS-MWA, W. Lafayette, IN.

Gee, D.M., Anderson, M.G., Baird, L., 1990. Large-scale floodplain modelling. Earth Surface Processes and Landforms 15, 513–523.

Heim, J.K., Warwick, J.J., 1997. Simulating sediment transport in the Carson River and Lahontan Reservoir, Nevada. Journal of the American Water Resources Association 33(1), 177–191.

Henderson, F.M., 1966. Open Channel Flow, Prentice-Hall Inc, Upper Saddle River, NJ.

Hoffman, R.J., Taylor, R.L., 1998. Mercury and suspended sediment, Carson River basin, Nevada, loads to and from Lahontan Reservoir in flood year 1997 and deposition in reservoir prior to 1983. FS-001-98, USGS.

Hosseinipour, E.Z., Martin, J.L., 1990. RIVMOD: A One-Dimensional Hydrodynamic Sediment Transport Model: Model Theory and User's Guide, USEPA, Athens, Georgia.

Howard, A.D., 1992. Modeling channel migration and floodplain sedimentation in meandering streams. In: Carling, P.A., Petts, G.E. (Eds.), Lowland Floodplain Rivers: Geomorphological Perspectives, Wiley, Chichester, pp. 1–41.

Johnson, B.E., Julien, P.Y., Molnar, D.K., Watson, C.W., 2000. The two-dimensional upland erosion model CASC2D-SED. Journal of the American Water Resources Association 36(1), 31–42.

Katzer, T., Bennett, J.P., 1983. Sediment Transport Model for the East Fork of the Carson River, Carson Valley, Nevada, 1983 Symposium on Urban Hydrology, Hydraulics and Sediment Control, University of Kentucky, Lexington, Kentucky, July 25–28, 1983, pp. 421–435.

Meade, J.R., 1990. Movement and storage of sediment in rivers of the United States and Canada. In: Wolman, M.G., Riggs, H.C. (Eds.), Surface Water Hydrology. The Geology of North America, Geological Society of America, Boulder, CO, pp. 255–280.

Miller, J.R., Lechler, P.J., Rowland, J., Desilets, M., Hsu, L.C., 1995. An integrated approach to the determination of the quantity, distribution, and the dispersal of mercury in Lahontan Reservoir, Nevada, USA. Journal of Geochemical Exploration 52, 45–55.

Miller, J.R., Lechler, P.J., Desilets, M., 1998. The role of geomorphic processes in the transport and fate of mercury in the Carson River basin, west-central Nevada. Environmental Geology 33(4), 249–262.

Miller, J.R., Barr, R., Grow, D., Lechler, P., Richardson, D., Waltman, K., Warwick, J., 1999. Effects of the 1997 flood on the transport and storage of sediment and mercury within the Carson River valley, west-central Nevada. Journal of Geology 107(3), 313.

Mount, J.F., 1995. California Rivers and Streams: the Conflict Between Fluvial Process and Land Use, University of California Press, Berkeley, CA, pp. 38–50.

Nicholas, A.P., Walling, D.E., 1998. Numerical modelling of floodplain hydraulics and suspended sediment transport and deposition. Hydrological Processes 12, 1339–1355.

Pizzuto, J.E., 1987. Sediment diffusion during overbank flows. Sedimentology 34, 301–317.

Smith, G.H., Tingley, J.V., 1998. The History of the Comstock Load, 1850–1997, Nevada Bureau of Mines and Geology in Association with the University of Nevada Press.

Thomann, R.V., Mueller, J.A., 1987. Principles of Surface Water Quality Monitoring and Control, Harper Collins Publishers, Inc, New York, NY, 549 p..

Walling, D.E., He, Q., 1997. Investigating spatial patterns of overbank sedimentation of river floodplains. Water, Air and Soil Pollution 99, 9–20.

Warwick, J.J., Heim, K.J., 1995. Hydrodynamic modeling of the Carson River and Lahontan Reservoir, Nevada. Water Resources Bulletin 31(1), 67–77.